Journal of Magnetic Resonance 212 (2011) 426–430

Contents lists available at SciVerse ScienceDirect

Journal of Magnetic Resonance

journal homepage: www.elsevier.com/locate/jmr

Non-uniformity correction of human brain imaging at high field by RF field mapping of B_1^+ and B_1^-

Hidehiro Watanabe *, Nobuhiro Takaya, Fumiyuki Mitsumori

Center for Environmental Measurement and Analysis, National Institutes for Environmental Studies, 16-2 Onogawa, Tsukuba, Ibaraki 305-8506, Japan

ARTICLE INFO

Article history:
Received 11 April 2011
Revised 28 July 2011
Available online 11 August 2011

Keywords:
High field
Non-uniformity
Human brain
RF field

ABSTRACT

A new method of non-uniform image correction is proposed. Image non-uniformity is originated from the spatial distribution of RF transmission and reception fields, represented as B_1^+ and B_1^-, respectively. In our method, B_1^+ mapping was performed *in vivo* by a phase method. In B_1^- mapping, images with multiple TEs were acquired with a multi-echo adiabatic spin echo (MASE) sequence which enables homogeneous excitation. By T_2 fitting of these images an M_0 map (M_0^{MASE}) was obtained, in which signal intensity was expressed as the product of B_1^- and $M_0(1-e^{-TR/T_1})$. The ratio of this M_0^{MASE} map to the B_1^+ map showed a similar spatial pattern in different human brains. These ratios of M_0^{MASE} to B_1^+ in 24 subjects were averaged and then fitted with a spatially polynomial function to obtain a ratio map of $B_1^-/B_1^+(\alpha)$. Uniform image was achieved in spin echo (SE), MASE and inversion recovery turboFLASH (IRTF) images using measured B_1^+ and calculated B_1^- by αB_1^+. Water fractions in gray and white matters obtained from the M_0 images corrected by this method were in good agreement with previously reported values. From these experimental results, the proposed method of non-uniformity correction is validated at 4.7 T imaging.

1. Introduction

Images obtained at high magnetic field strengths are advantageous in high sensitivity and good spatial resolution, but suffer from non-uniform signal intensity, which could cause difficulties in quantitative image analyses. For example, human brain segmentation is sensitive to non-uniform image intensities. Thus, several post-processing methods such as fitting with polynomial or Bayesian functions have been proposed [1,2]. This non-uniformity is caused by B_1 inhomogeneity derived from RF interference effects and from RF coil imperfections. It has been reported that transmission and reception fields were represented as $\boldsymbol{B}_1^+$ and $\boldsymbol{B}_1^{-*}$, respectively where these are complex vectors and * denotes complex conjugate [3,4]. These fields differ in spatial distribution even with a transceiver RF coil in human brain imaging at high field where wavelength at Larmor frequency is comparable to or even less than sample size [5–7]. Then, B_1^+ and B_1^- maps which are magnitude of $\boldsymbol{B}_1^+$ and $\boldsymbol{B}_1^{-*}$, respectively, are indispensable for non-uniformity corrections of MR images in this case. Several measurement methods such as double-angle techniques [8] or phase methods [9] have been reported to obtain a transmission field map. Reception field mapping has been reported in parallel imaging methods for separate RF coils for transmission and reception [10]. At high field these reception fields cannot be measured for transceiver coils, because the obtained images are always associated with the proton density. Then, these field maps have not been well pursued except for the estimation method proposed by Wang et al. with minimum contrast condition [11].

In this work, we propose a new approach to calculate a B_1^- map semi-empirically by a measured B_1^+ map in a human brain. We compared M_0 maps obtained from MASE images with homogeneous excitation by adiabatic pulses and measured B_1^+ maps among various human brains. Ratio maps of M_0^{MASE} to B_1^+ in various human brains turned out to be similar by a visual inspection. Then, we thought that the B_1^- map could be calculated by a ratio map α and a B_1^+ map obtained in each brain. All the human brain images obtained by MASE, ordinary SE, and IRTF were reasonably corrected by this method. Further, fractions of water content (f_w) in various regions measured on the corrected M_0 maps were in good agreement with the literature values.

2. Methods

2.1. Measurements of RF field maps in human brains

Human brain measurements were performed on six healthy male (44 ± 14 years) and 18 healthy female (41 ± 12 years) subjects. Images on a 2D slice plane across the basal ganglia were acquired after obtaining informed consent following a protocol approved by the institutional review board at the National Institute for Environmental Studies. The measurements were performed

* Corresponding author. Fax: +81 29 850 2880.
E-mail address: hidewata@nies.go.jp (H. Watanabe).

1090-7807/$ - see front matter © 2011 Elsevier Inc. All rights reserved.
doi:10.1016/j.jmr.2011.08.001

using a 4.7 T whole-body NMR spectrometer (*INOVA*, Agilent). A quadrature TEM coil with a diameter of 300 mm was used for both transmission and reception.

In B_1^+ measurements by a phase method [9], a set of two spin echo (SE) images were acquired using hyperbolic secant (HS) pulses for both excitation and refocusing on the same slice plane with TR/TE of 500/30 ms. Frequency sweep of those pulses was applied in the opposite direction in the two acquisitions. When duration of the $\pi/2$ HS pulse is twice as that of the π pulse, a B_1^+ map can be calculated from the phase difference obtained from those two images. Durations of $\pi/2$ and π pulses were 12 ms and 6 ms, respectively. Bandwidth in both pulses was 1.6 kHz. The number of acquisitions was two with a matrix size of 256×128; the measurement time was 4 min per set of two SE images. For B_1^- mapping, six images were acquired by a MASE [12,13] sequence with TR/TE of 4000/26, 52, 78, 104, 130, and 156 ms in a measurement time of 17 min. Other conditions were the same as we previously reported. By fitting a single exponential curve using Eq. (1) to the signal intensity of each pixel in the six MASE images, M_0^{MASE} and T_2 maps were generated.

$$S = M_0^{\mathrm{MASE}} \mathrm{e}^{-\mathrm{TE}/T_2} \tag{1}$$

Signal intensities on the obtained M_0^{MASE} image are expressed as

$$M_0^{\mathrm{MASE}} = M_0(1 - \mathrm{e}^{-\mathrm{TR}/T_1})B_1^- \tag{2}$$

Since M_0 is proportional to water content, the intensity of M_0^{MASE} can be considered as B_1^- attenuated by small tissue-dependent differences in water content and T_1. Ratio maps of M_0^{MASE} divided by B_1^+ were calculated in individual subjects and compared to investigate relationship between B_1^+ and B_1^- maps.

2.2. Ratio map of $M_0^{\mathrm{MASE}}/B_1^+$

Ratio maps of $M_0^{\mathrm{MASE}}/B_1^+$ in human brains appeared a similar spatial pattern among various subjects (Fig. 1a). From this experimental findings, we hypothesized that B_1^- could be approximated as follows:

$$B_1^-(\mathbf{x}) \sim \alpha(\mathbf{x}) B_1^+(\mathbf{x}) \tag{3}$$

where $B_1^+ = |\boldsymbol{B}_1^+|$ and $B_1^- = |\boldsymbol{B}_1^{-*}|$ and the ratio of B_1^-/B_1^+ was denoted as the ratio map, $\alpha(\mathbf{x})$ which is a function varying spatially among various brains in measurements with the particular TEM coil used in this study. If we get an adequate α map empirically, non-uniformity correction only requires a B_1^+ map under the hypothesis of $B_1^- \sim \alpha B_1^+$. For obtaining the α map, we calculated a $\left\langle M_0^{\mathrm{MASE}}/B_1^+ \right\rangle_{\mathrm{ave}}$ map averaged from 24 subjects to avoid individual differences. Brains were set in a similar location inside the TEM coil in all subjects and all maps of $M_0^{\mathrm{MASE}}/B_1^+$ were merely averaged without any post-processing protocols such as co-registration or deformation. Fig. 1 shows a $\left\langle M_0^{\mathrm{MASE}}/B_1^+ \right\rangle_{\mathrm{ave}}$ map (b) and a trimmed map (c). That averaged trimmed map was fitted with a polynomial function of the 7th degree on a 2D space to smooth tissue dependent M_0 differences. Then, we regarded the generated map as the α map (Fig. 1d).

2.3. Non-uniformity corrections in human brain images

Non-uniformity corrections were performed by measured B_1^+ and calculated B_1^- maps with Eq. (3) on the M_0^{MASE} maps and the SE magnitude images obtained in the B_1^+ measurements to validate our technique. For corrections of SE images we used Eq. (4) derived from Eq. (1) when $\beta_{\mathrm{SE}} = 2\alpha_{\mathrm{SE}}$ in Wang's literature [11]. Note that Eq. (1) lacks term of $(1 - \cos\beta_{\mathrm{SE}}(x))/2$ [11].

$$S_{SE} = M_0 B_1^- \sin^3\theta \mathrm{e}^{-\mathrm{TE}/T_2} f(T_1, \mathrm{TR}, \theta) \tag{4}$$

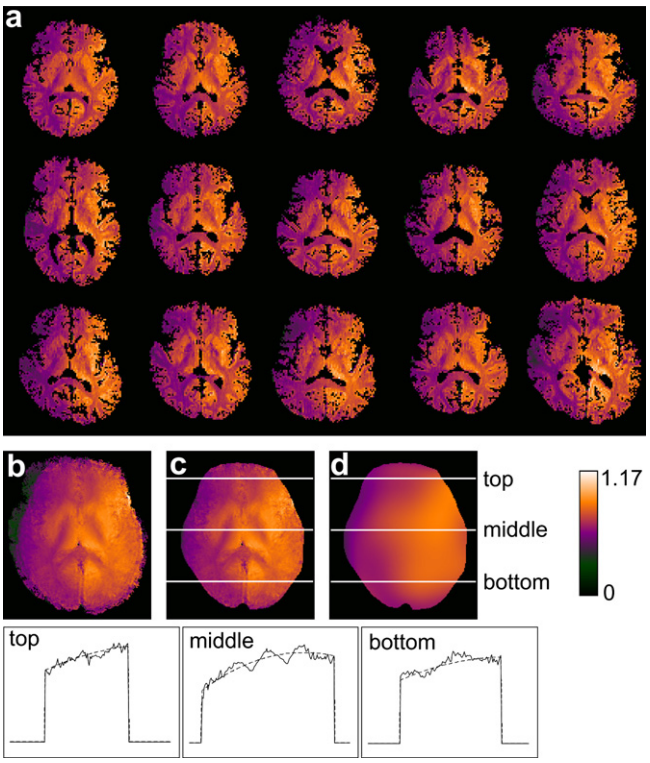

Fig. 1. $M_0^{\mathrm{MASE}}/B_1^+$ maps in 15 subjects (a). M_0^{MASE} maps was generated by removing CSF after fitting MASE images with multiple TEs. These $M_0^{\mathrm{MASE}}/B_1^+$ maps appeared to have similarity in spatial patterns among subjects. The maps of $\left\langle M_0^{\mathrm{MASE}}/B_1^+ \right\rangle_{\mathrm{ave}}$ averaged over 24 subjects (b). A ratio map $\alpha(\mathbf{x})$ (d) was generated by fitting the averaged map (c) after trimming the peripheral regions with a polynomial function of the 7th degree on a 2D space. Profiles along the top, middle and bottom lines in the trimmed averaged map (solid line) and those in the α map (broken line) are also shown.

$$\theta = \frac{\pi}{2}\frac{B_1^+}{B_{1\ \mathrm{ref}}^+} \tag{5}$$

$$f(T_1, \mathrm{TR}, \theta) = \frac{1 - \mathrm{e}^{-\mathrm{TR}/T_1}\mathrm{e}^{\mathrm{TE}/2T_1} - (1 - \mathrm{e}^{\mathrm{TE}/2T_1})\mathrm{e}^{-\mathrm{TR}/T_1}\cos(2\theta)}{1 - \mathrm{e}^{-\mathrm{TR}/T_1}\cos\theta\cos(2\theta)} \tag{6}$$

where $B_{1\ \mathrm{ref}}^+$ is a transmission field at flip angle of $\pi/2$.

We also corrected M_0 maps calculated from IRTF images (M_0^{IRTF}). In these measurements, images were collected with multiple inversion times (TI) of 10, 100, 200, 400, 800, 1600, 3200, 6400, and 15,000 ms. An adiabatic pulse, called an HS1 pulse, with a duration of 8 ms and BW of 1.2 kHz was used as an inversion pulse. A one-side-lobe sinc pulse of 2 ms was used for excitation with a flip angle of 10°. A data matrix of 256×256 was collected with a two-segmented centric order scheme with a relaxation delay of 15 s to meet the full longitudinal relaxation. Image contrast is mostly contained in center of k-space, which occurs at TI delay after fully relaxed magnetization is completely inverted by the IR adiabatic pulse. TR/TE was 9/4 ms and, slice thickness was 2.5 mm in all measurements. A TE of 4 ms gives a negligible T_2^* decay. Under a low flip angle of $\theta = 10°$, $\sin\theta$ is approximately equals to θ and B_1^+ is proportional to θ. Then, signal intensities on IRTF images, affected only by an inhomogeneous transmission field of B_1^+, are expressed as

$$S = M_0^{\mathrm{IRTF}}(1 - 2\mathrm{e}^{-\mathrm{TI}/T_1}) \tag{7}$$

$$M_0^{\mathrm{IRTF}} = M_0 B_1^- B_1^+ \tag{8}$$

By fitting an exponential curve using Eq. (7) to the signal intensity of each pixel in the nine IRTF images, M_0^{IRTF} and T_1 maps were generated. M_0^{IRTF} maps were corrected by Eq. (8).

2.4. Measurements of regional fractions of water content

To measure water content, a B_1^--corrected M_0^{MASE} image was further corrected by Eq. (2) using a measured T_1 map, generating an M_0 image. Signal intensities in six regions of caudate, putamen, thalamus, globus pallidus, frontal cortex and frontal white matter were measured in both the right and left hemispheres on an M_0 image and the averaged values of the intensities were defined as signal intensity S in the corresponding region. Each region was selected to avoid partial volume errors along the axial direction by the same procedure as we previously reported [13,14]. The fraction of water content, f_w, was calculated using S, the average of S in six regions, S^{av}, and the average of the previously reported f_w in the above six regions [14,15], f_w^{av}, as follows:

$$f_w = \frac{S}{S^{av}} f_w^{av} \tag{9}$$

3. Results

3.1. Non-uniformity correction in human brain images

SE images, M_0^{MASE} and M_0^{IRTF} maps were individually corrected using measured B_1^+ maps and calculated B_1^- maps by αB_1^+. Fig. 2

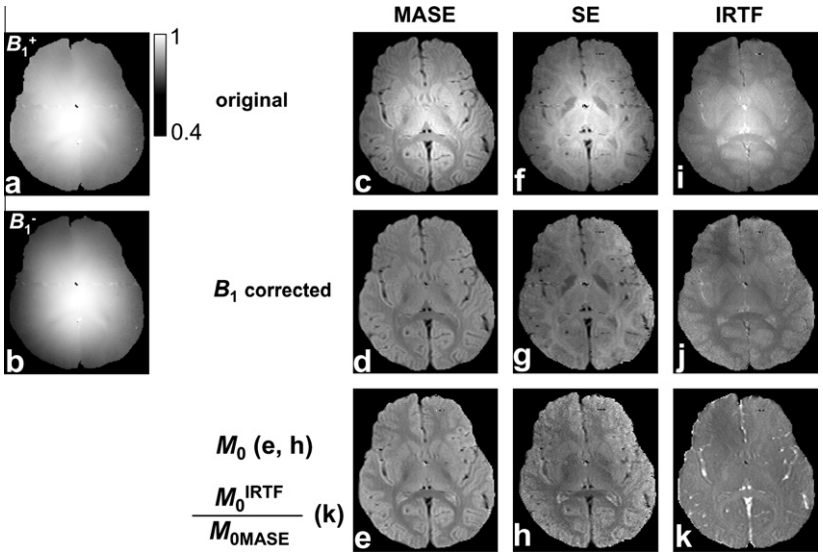

Fig. 2. Non-uniformity correction of various images obtained from a single subject using both B_1^+ (a) and B_1^- (b) maps. An M_0^{MASE} map (c) was generated after fitting the MASE images with multiple TEs. A more uniform map was obtained after B_1^- correction (d). (e) T_1-corrected M_0 map from (d). Original, B_1^+ and B_1^- corrected, and T_1 and T_2 corrected images (f, g, h) in SE measurements. The B_1^- corrected image was calculated by removing B_1^- $\sin^3\theta$(g). Original, and B_1^+ and B_1^- corrected maps in IRTF measurements (i, j). A B_1-corrected M_0^{IRTF} map (j) without relaxation effects was equal to an M_0 map. (k) Ratio of (j)–(e).

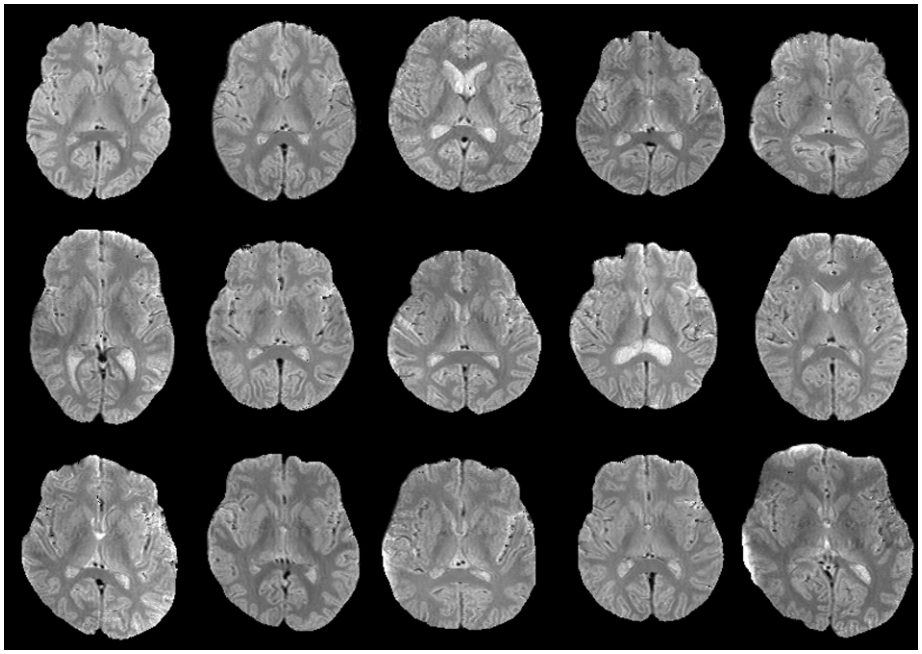

Fig. 3. M_0 maps corrected from M_0^{MASE} maps in 15 subjects. Almost uniform maps appeared in all subjects.

shows both B_1^+ and B_1^- maps, and brain images in one subject before and after the B_1 correction. The central regions of human brains had higher intensities in the M_0^{MASE} map before correction (Fig. 2c) due to inhomogeneous RF field distributions. After the B_1 correction, the central higher intensities disappeared and the map became more uniform (Fig. 2d). The signal intensities in this corrected map should be expressed by $M_0(1-e^{-TR/T_1})$ and give an M_0 map by dividing with a relaxation term $1-e^{-TR/T_1}$ (Fig. 2e).

Higher signal intensities in central regions also appeared in original SE image (Fig. 2f) and M_0^{IRTF} map (Fig. 2i). Compared with the M_0^{MASE} image, the distribution patterns were more sharply curved due to the effect of B_1^+ and B_1^- in the SE image and the M_0^{IRTF} map (see Eqs. (4) and (8)). After the corrections by B_1^+ and B_1^-, brighter spots in the central regions also disappeared in the SE image (Fig. 2g) and M_0^{IRTF} map (Fig. 2j). However, asymmetric signal intensities remained especially in the right peripheral region in the SE image (Fig. 2g) and in the left region in the M_0^{IRTF} map (Fig. 2j). These may be caused by error in B_1^+, which leads to overcorrection in the SE image and the M_0^{IRTF} map.

Fig. 2h shows M_0 map calculated from B_1-corrected SE image by removing $f(T_1, TR, \theta)$ and T_2 terms. Since an M_0^{IRTF} map is not affected by T_1 and T_2, B_1-corrected M_0^{IRTF} map (Fig. 2j) is equal to an M_0 map. The M_0 map from the SE image (Fig. 2h) had almost similar distributions to the M_0 map from MASE (Fig. 2e) except high intensities in the right peripheral regions due to B_1^+ error and a noisy image. That noise was enhanced by fairly substantial T_1 correction due to TR = 500 ms, comparing with limited changes to the MASE images with TR = 4000 ms.

Higher CSF signals are conspicuous in the division image (Fig. 2k) of the M_0 map from IRTF (Fig. 2j) by that from MASE (Fig. 2e). While CSF signals were not suppressed because of centric order scheme, relaxation delay of 15 s and short TE = 4 ms in IRTF measurements, they might be diminished due to flow voids in the MASE sequence [12,13] where read and phase encoding gradients are not rewinded. Flow voids might decrease CSF signals also in the M_0 map from SE (Fig. 2h). Fig. 3 shows M_0 maps in 15 subjects corrected from M_0^{MASE} map. We confirmed that $B_1^-(\mathbf{x})$ could be calculated by $\alpha(\mathbf{x})B_1^+(\mathbf{x})$ form these uniform maps.

3.2. Measurements of regional fractions of water content

The mean and standard deviation values of f_w measured on the corrected M_0 images from 22 subjects from MASE measurements were plotted in Fig. 4 with previously reported values [14,15]. The measured values were in good agreement with the reported ones. Our proposed method of non-uniformity correction using B_1^+ and B_1^- was validated by the obtained f_w values as well as by the uniform images after the correction.

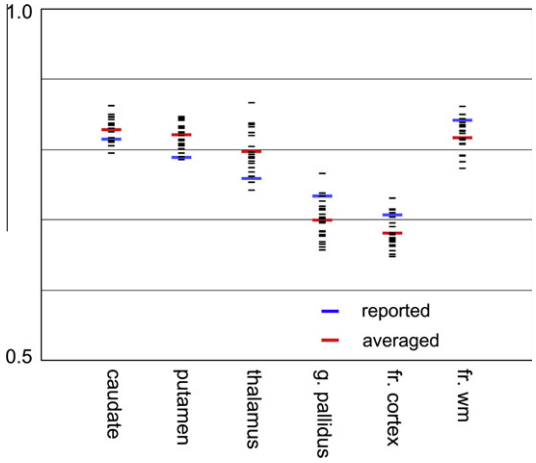

Fig. 4. Measured fractions of water contents in various regions of human brain. Data of 22 subjects along with averaged data in 22 subjects (blue bar) and reported data (red bar). g. pallidus, glubus pallidus; fr. cortex, frontal cortex; fr. wm, frontal white matter. (For interpretation of the references to colour in this figure legend, the reader is referred to the web version of this article.)

4. Discussion

MRI signal intensity, S is primarily determined by M_0, relaxation and B_1^+ terms $f(T_1, T_2, \int(\gamma B_1^+ t)dt)$, and B_1^-.

$$S = M_0 B_1^- f\left(T_1, T_2, \int(\gamma B_1^+ t)dt\right) \tag{10}$$

Since B_1^+ and B_1^- differ in spatial distribution at high field, both field maps *in vivo* are required to correct non-uniform images. Several methods have been reported to measure B_1^+ maps. One is the double-angle method using amplitude modulation [8] and another is the phase method [9]. In double-angle methods a B_1^+ map is calculated from a comparison of magnitudes using at least two images obtained by different flip angles and a long TR is required to avoid T_1 partial saturation effects. We used a phase method, where the shorter TR is applicable.

Wang calculated a B_1^- map using measured B_1^+ with minimized contrasts by choosing adequate TR and TE at 128 MHz which is Larmor frequency of proton at 3 T. Since S is roughly a product of B_1^- and $f(\int(\gamma B_1^+ t)dt)$ under this condition without M_0, T_1 and T_2, B_1^- is approximated by dividing the image with $f(\int(\gamma B_1^+ t)dt)$. To eliminate any remaining non-uniformity due to contrast differences among tissues, a low-pass filter was applied spatially. Compared to their method, we hypothesized that B_1^- could be calculated by αB_1^+ from the experimental findings with the particular TEM coil at 200 MHz (Fig. 1) where the ratio map of α was obtained from the MASE measurements. Non-uniformity was successfully corrected in either SE, MASE or IRTF measurement of human brains by the calculated B_1^- map. The hypothesized relationship of $B_1^- \sim \alpha(\mathbf{x}B_1^+)$ is validated by this result as well as by the obtained f_w that was consistent with previously reported values. It should be noted that this relationship could be applied with a transceiver quadrature volume coil where phases of two feeding ports at reception differ from those at transmission. This might be because those phases are fixed among subjects. This proposed method cannot be applied to a transceiver array coil when RF phase and amplitude of each coil element is adjusted for each subject by RF shimming.

B_1^- map could be calculated by this ratio map $\alpha(\mathbf{x})$ and the non-uniformity correction in human brain imaging could be done only by B_1^+ measurement in a short measurement time. When $\alpha(\mathbf{x})$ is obtained in 3D spaces inside a volume coil, this correction could be applied to 3D images. The ratio map α can be used for a subject in spine position from the experimental results that fairly uniform images could be achieved in all subjects (Fig. 3). It is necessary to evaluate whether this method can be applied to diseases.

Reception field mapping is one of the key technologies in parallel imaging methods [10] using separate RF coils for transmission and reception. In this method, images are obtained by a surface coil with body coil transmission. A reference image on the same slice is also acquired by the body coil for both transmission and reception. Then, a sensitivity map can be calculated from the ratio of the surface coil image to reference image. In this case, the signal intensities are

$$S_{T/R} = M_0 B_{1\ receive}^- f\left(T_1, T_2, \int(\gamma B_{1\ transmit}^+ t)dt\right) \tag{11}$$

$$S_{T\&R} = M_0 B_{1\ transmit}^- f\left(T_1, T_2, \int(\gamma B_{1\ transmit}^+ t)dt\right) \tag{12}$$

In these expressions, $B_{1\ \mathrm{transmit}}^{+}$ and $B_{1\ \mathrm{transmit}}^{-}$ are B_1^+ and B_1^- of the body coil for transmission and $B_{1\ \mathrm{receive}}^{-}$ is B_1^- of the surface coil for reception. $S_{\mathrm{T/R}}$ is signal intensity obtained by surface coil detection and $S_{\mathrm{T\&R}}$ is that of reference image. Using these equations, signal intensity on the sensitivity map is written as

$$S_{\mathrm{sensitivity\_map}} = \frac{S_{\mathrm{T/R}}}{S_{\mathrm{T\&R}}} = \frac{B_{1\ \mathrm{receive}}^{-}}{B_{1\ \mathrm{transmit}}^{-}} \tag{13}$$

The sensitivity map commonly used in parallel imaging is less affected by $B_{1\ \mathrm{transmit}}^{-}$ especially at 1.5 T. However, $B_{1\ \mathrm{transmit}}^{-}$ should be corrected at a field higher than 3 T. In this case, our findings of $B_{1\ \mathrm{transmit}}^{-} \sim \alpha B_{1\ \mathrm{transmit}}^{-}$ might be applicable, although α should be acquired for each transmission coil.

In conclusions, a B_1^- map can be approximated using an experimentally obtained B_1^+ map with a volume coil at 200 MHz. Image non-uniformity in human brain at high field can be corrected using these B_1^+ and B_1^- maps.

Acknowledgments

We thank Dr. Jang-Yeon Park for discussion on B_1^+ measurements by a phase method.

References

[1] J. Ashburner, K.J. Friston, Unified segmentation, NeuroImage 26 (2005) 839–851.
[2] J.T. Vaughan, M. Garwood, C.M. Collins, W. Liu, L. DelaBarre, G. Adriany, P. Andersen, H. Merkle, R. Goebel, M.B. Smith, K. Uğurbil, 7 T vs. 4 T: RF power, homogeneity, and signal-to-noise comparison in head images, Magn. Reson. Med. 46 (2001) 24–30.
[3] G.H. Glover, C.E. Hayes, N.J. Pelc, W.A. Edelstein, O.M. Mueller, H.R. Hart, C.J. Hardy, M. O'Donnell, W.D. Barber, Comparison of linear and circular polarization for magnetic resonance imaging, J. Magn. Reson. 64 (1985) 255–270.
[4] D.I. Hoult, The principle of reciprocity in signal strength calculations – a mathematical guide, Concepts Magn. Reson. 12 (2000) 173–183.
[5] C.M. Collins, Q.X. Yang, J.H. Wang, X. Zhang, H. Liu, S. Michaeli, X.-H. Zu, G. Adriany, J.T. Vaughan, P. Anderson, H. Merkle, K. Uğurbil, M.B. Smith, W. Chen, Different excitation and reception distributions with a single-loop transmit–receive surface coil near head-sized spherical phantom at 300 MHz, Magn. Reson. Med. 47 (2002) 1026–1028.
[6] J. Wang, Q.X. Yang, X. Zhang, C.M. Collins, M.B. Smith, X.-H. Zhu, G. Adriany, K. Uğurbil, W. Chen, Polarization of the RF field in a human head at high field: a study with a quadrature surface coil at 7.0 T, Magn. Reson. Med. 48 (2002) 362–369.
[7] P.F. van de Moortele, C. Akgun, G. Adriany, S. Moeller, J. Ritter, C.M. Collins, m.B. Smith, J.T. Vaughan, K. Uğurbil, B_1 destructive interferences and spatial phase patterns at 7 T with a head transceiver array coil, Magn. Reson. Med. 54 (2005) 1503–1518.
[8] J.P. Hornak, J. Szumowski, R.G. Bryant, Magnetic field mapping, Magn. Reson. Med. 6 (1988) 158–163.
[9] J.Y. Park, M. Garwood, B_1 mapping using phase information created by frequency-modulated pulses, in: Proceedings of the 16th Annual Meeting ISMRM, Tronto, Canada, 2008, p. 361.
[10] K.P. Pruessmann, M. Weiger, M.B. Scheidegger, P. Boesiger, SENSE: sensitivity encoding for fast MRI, Magn. Reson. Med. 42 (1999) 952–962.
[11] J. Wang, M. Qiu, Q.X. Yang, M.B. Smith, R.T. Constable, Measurement and correction of transmitter and receiver induced nonuniformities *in vivo*, Magn. Reson. Med. 53 (2005) 408–417.
[12] F. Mitsumori, H. Watanabe, N. Takaya, M. Garwood, Apparent transverse relaxation rate in human brain varies linearly with tissue iron concentration at 4.7 T, Magn. Reson. Med. 58 (2007) 1054–1060.
[13] F. Mitsumori, H. Watanabe, N. Takaya, Estimation of brain iron concentration in vivo using a linear relationship between regional iron and apparent transverse relaxation rate of the tissue water at 4.7 T, Magn. Reson. Med. 62 (2009) 1326–1330.
[14] O. Lowell, L.O. Randall, Chemical topography of the brain, J. Biol. Chem. 124 (1938) 481–488.
[15] N. Gelman, J.R. Ewing, J.M. Gorell, E.M. Spickler, E.G. Solomon, Interregional variation of longitudinal relaxation rates in human brain at 3.0 T: relaxation to estimated iron and water contents, Magn. Reson. Med. 45 (2001) 71–79.